

Research papers

Impact of the bottom drag coefficient on saltwater intrusion in the extremely shallow estuary

Hanghang Lyu, Jianrong Zhu*

State Key Laboratory of Estuarine and Coastal Research, East China Normal University, North Zhongshan Rd. 3663, Shanghai 200062, PR China



ARTICLE INFO

Article history:

Received 4 August 2017

Received in revised form 16 November 2017

Accepted 5 January 2018

Available online 6 January 2018

This manuscript was handled by Corrado Corradini, Editor-in-Chief, with the assistance of Magdeline Laba, Associate Editor

Keywords:

Saltwater intrusion
Bottom drag coefficient
Numerical model
Skill assessment
Changjiang Estuary

ABSTRACT

The interactions between the extremely shallow, funnel-shaped topography and dynamic processes in the North Branch (NB) of the Changjiang Estuary produce a particular type of saltwater intrusion, saltwater spillover (SSO), from the NB into the South Branch (SB). This dominant type of saltwater intrusion threatens the winter water supplies of reservoirs located in the estuary. Simulated SSO was weaker than actual SSO in previous studies, and this problem has not been solved until now. The improved ECOM-si model with the advection scheme HSIMT-TVD was applied in this study. Logarithmic and Chézy-Manning formulas of the bottom drag coefficient (BDC) were established in the model to investigate the associated effect on saltwater intrusion in the NB. Modeled data and data collected at eight measurement stations located in the NB from February 19 to March 1, 2017, were compared, and three skill assessment indicators, the correlation coefficient (CC), root-mean-square error (RMSE), and skill score (SS), of water velocity and salinity were used to quantitatively validate the model. The results indicated that the water velocities modeled using the Chézy-Manning formula of BDC were slightly more accurate than those based on the logarithmic BDC formula, but the salinities produced by the latter formula were more accurate than those of the former. The results showed that the BDC increases when water depth decreases during ebb tide, and the results based on the Chézy-Manning formula were smaller than those based on the logarithmic formula. Additionally, the landward net water flux in the upper reaches of the NB during spring tide increases based on the Chézy-Manning formula, and saltwater intrusion in the NB was enhanced, especially in the upper reaches of the NB. At a transect in the upper reaches of the NB, the net transect water flux (NTWF) is upstream in spring tide and downstream in neap tide, and the values produced by the Chézy-Manning formula are much larger than those based on the logarithmic formula. Notably, SSO during spring tide was 1.8 times larger based on the Chézy-Manning formula than that based on the logarithmic formula. The model underestimated SSO and salinity at the hydrological stations in the SB based on the logarithmic BDC formula but successfully simulated SSO and the temporal variations in salinity in the SB using the Chézy-Manning formula of BDC.

© 2018 Elsevier B.V. All rights reserved.

1. Introduction

In single-channel estuaries, saltwater intrusion generally develops in the along-channel direction. However, in bifurcated estuaries, lateral saltwater intrusion may be significant and can play an important role in determining the temporal variation and spatial distribution of salinity in the spring-neap tidal cycle (Wu et al., 2006; Gong and Shen, 2011; Wang et al., 2012). The Changjiang, also known as the Yangtze River, is one of the largest rivers in the world. The Changjiang Estuary has a 90-km-wide river mouth and is characterized by multiple bifurcations (Fig. 1). Firstly, the

estuary is divided by Chongming Island into the South Branch (SB) and North Branch (NB). The SB and its lower reaches form the main channel of the Changjiang and contribute to the majority of river discharge, while the NB is heavily silted. Secondly, the lower SB is bifurcated into the South Channel (SC) and the North Channel (NC) by Changxing Island and Hengsha Island. Finally, the SC is bifurcated into the South Passage (SP) and the North Passage (NP) by Jiuduansha Island. According to water column stratification or vertical salinity structure, estuaries can be divided into three categories: type A (salt wedge or strongly stratified), type B (partially mixed), and type C (vertically well mixed) (Prichard, 1955; Cameron and Prichard, 1963). Shen et al. (2003) concluded that the NB and SB belong to the type C, and the NC, NP and SP present as type B during spring tide and present as type A during neap

* Corresponding author.

E-mail address: jrzhu@sklec.ecnu.edu.cn (J. Zhu).

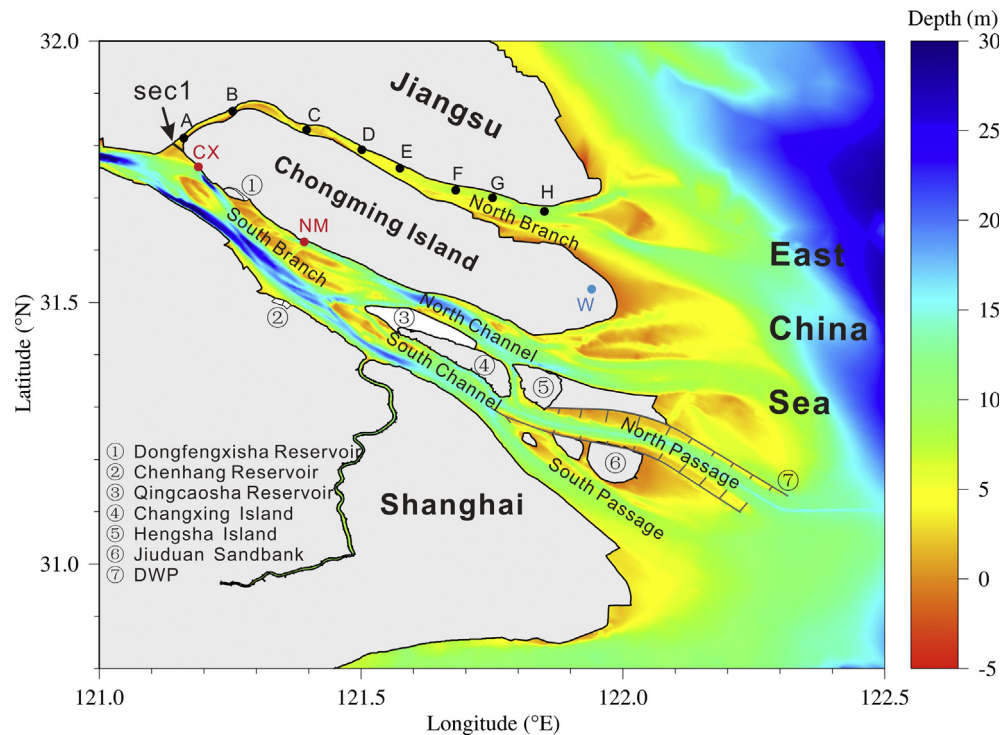


Fig. 1. Topography of the Changjiang Estuary. Black dots indicate the locations of measurement stations in February 2017; red dots indicate the locations of hydrologic stations Nanmen (NM) and Chongxi (CX); sec1 is a transect located in the inlet of the NB; W is the location of the weather station at the Chongming eastern shoal; and DWP is the Deep Waterway Project. (For interpretation of the references to colour in this figure legend, the reader is referred to the web version of this article.)

tide. Saltwater intrusion in the Changjiang Estuary is mainly controlled by the river discharge and tide (Shen et al., 2003; Wu et al., 2006; Li et al., 2010; Zhu et al., 2010; Qiu et al., 2012) but is also influenced by wind (Li et al., 2012), topography (Li, et al., 2014), river basin and estuarine projects (Zhu, et al., 2006; Qiu and Zhu, 2013) and sea level rise (Qiu and Zhu, 2015). River discharge is recorded at the Datong gauge station, which is located 620 km from the Changjiang mouth. Discharge exhibits pronounced seasonal variations, with the lowest monthly mean value of $11,200 \text{ m}^3\text{s}^{-1}$ in January and the highest monthly mean value of $49,700 \text{ m}^3\text{s}^{-1}$ in July (Changjiang Water Resources Commission, based on data from 1950 to 2016). The tides in the estuary exhibits semidiurnal, diurnal, and fortnightly spring-neap signals (Zhu, et al., 2015).

The natural evolution and artificial reclamation of the intertidal zone from the 1950s to 2000s has severely narrowed the upper reaches of the NB (Zhu and Bao, 2016). Consequently, the upper reaches of the NB have become almost orthogonal to the SB, while the lower reaches have become funnel shaped. The evolution of the river regime of the NB has helped to prevent runoff from entering the NB, especially during the dry season, was also making the tidal range larger in the NB than in the SB. Strong tidal forcing in the NB induces significant subtidal circulation, resulting in a net landward flow when river discharge is low during spring tide (Wu et al., 2006; Xue et al., 2009). This residual transport forms a type of saltwater intrusion known as saltwater spillover (SSO) from the NB into the SB, which is the most characteristic type of saltwater intrusion in the estuary. During spring tide, the water level rises considerably in the upper reaches of the NB due to its funnel shape, leading to a massive amount of SSO from the shoals into the SB. Only a small amount of the saltwater returns to the NB because the shoals in the upper reaches of the NB are exposed to the air during ebb tide. The saltwater that is spilled into the SB is transported downstream by runoff and arrives in the middle reaches

of the SB during the subsequent neap tide. This process impacts Dongfengxisha Reservoir, Chenhang Reservoir and Qingcaosha Reservoir (QCSR) and threatens Shanghai's water supply. The massive QCSR was built in 2010 along the northwestern portion of Changxing Island, and it supplies more than 70% of the freshwater for Shanghai. Water from the Changjiang is allowed to flow into QCSR when the salinity is lower than 0.45 (the salinity standard of drinking water), but this operation is suspended when saltwater intrusion influences the water intake.

Although the author's research group has conducted intensive studies of saltwater intrusion in the Changjiang Estuary, we found that the modeled SSO was weaker than the real situation, especially during spring tide. The mean topographic depth is 3.07, 3.44 and 5.07 m (here and throughout the manuscript, the datum is the mean sea level of the Yellow Sea) in the upper, middle and lower reaches of the NB, and tidal flats with depths of less than 2 m account for 39%, 23%, and 32% of these reaches, respectively. Therefore, the NB is extremely shallow. The bottom drag coefficient (BDC) determined by the law of the wall in previous studies may be unsuitable for the extremely shallow NB.

The BDC C_d is determined by the law of the wall, and the logarithmic profile can be obtained via integration (Batchelor, 1953).

$$\tau_b = \rho C_d |u_b| u_b \quad (1)$$

$$C_d = \left[\frac{1}{\kappa} \ln \left(\frac{z_b}{z_0} \right) \right]^{-2} \quad (2)$$

where τ_b is the bottom friction stress; C_d is the BDC; u_b is the bottom current velocity at z_b ; z_b is the height from the bottom; κ is the von Karman constant (equal to 0.4); and z_0 is the bottom roughness, which is set to 0.001 m in this study. In many studies, the structure of tidally induced flow in channels and embayments has been characterized as logarithmic (Dyer, 1980; Soulsby and Dyer, 1981; Lueck, 1988).

The logarithmic law of BDC C_d may be unsuitable for extremely shallow waters. Collins et al. (1998) analyzed 192 current velocity datasets collected from the tidal flats of the Loughor Estuary, Swansea Bay and Wash Bay and found that fewer than 40% of the datasets were logarithmic in character. In many previous studies of extremely shallow water, the BDC C_d has been written based on the Chézy-Manning formula (Dronkers, 1964; Ludwick, 1975; Dunbar et al., 1991; Bokhorst, 2003).

$$C_d = \frac{g}{C^2} \quad (3)$$

In this equation, C is the Chézy coefficient, which can be determined from the Manning roughness coefficient n (Chow, 1959).

$$C = \frac{\sqrt[6]{H}}{n} \quad (4)$$

where H is the water depth. Determining the value of the Manning roughness coefficient becomes the key issue in this calculation. Notably, the Manning roughness coefficient varies with depth in shallow waters. Ree (1981) found that the Manning roughness coefficient varied with the flow depth in a large number of flume experiments. Based on measurement data from gauge stations along the lower reaches of the Yellow River, Qian et al. (1959) concluded that the Manning roughness coefficient gradually decreased with increasing water level. Chow (1959) argued that an increase in flow depth would cause a decrease in the Manning roughness coefficient of most open channels. Knight (1981) and Knight et al. (2009) found that the Manning roughness coefficients of the Conwy Estuary, Main River, Severn River, Waiwakaiho River and Tomebamba River varied significantly with water stages through field measurements. Notably, the Manning roughness coefficient exhibited a decreasing trend with increasing tidal amplitude. Cheng et al. (1993) found that the model results achieved a best fit to field data when the value of the Manning roughness coefficient was assigned based on a range of water depths.

Saltwater intrusion can produce estuarine circulation (Pritchard, 1956) and effect stratification (Simpson et al., 1990), thereby influencing sediment transport, producing peak estuarine turbidities (Geyer, 1993), and degrading the quality of freshwater flowing into reservoirs in the Changjiang Estuary. Based on numerical experiments of BDC, we further studied saltwater intrusion in the NB to improve the simulation accuracy of SSO in this paper. The remainder of the paper is organized as follows. Section 2 describes field observations, the numerical model and experiments. In Section 3, the effect of the BDC on saltwater intrusion in the NB, as well as SSO, is analyzed and discussed. Finally, conclusions are presented in Section 4.

2. Methods

2.1. Observations

We conducted the field observations in the NB from February 19 to March 1, 2017. Eight measurement stations located along the NB were sampled (Fig. 1). We synchronously began the surveys at B, D, F and H stations (black solid circles in Fig. 1) during the neap (February 19–21, 2017, Fig. 2a) to cover 4 complete semidiurnal tidal cycles. The mean water depths of stations B, D, F and H were 2.80, 4.28, 6.14, and 8.02 m, respectively. One bottom-mounted tripod was placed at each of these stations, and one boat was secured close to each tripod. After the observations during the neap tide, we move the tripods and boats from stations B, D, F and H to stations A, C, E and G to conduct observations during the neap-middle-spring tide, which (February 21–27, 2017, Fig. 2a) lasted approximately 6 days. The mean water depths of stations A, C, E and G were 2.45, 2.65, 4.37, and 6.01 m, respectively. After this

observation period, we again moved the tripods and boats to stations B, D, F and H to conduct observations during the spring tide. Observations were collected (February 27–March 1, 2017, Fig. 2a) for at least 48 h to cover 4 complete semidiurnal tidal cycles.

At each measurement station, the tripod was mounted to the river bottom and equipped with instruments 0.2 m above the river bottom. A 600-kHz Acoustic Doppler Current Profiler (ADCP, RD Instruments) was used to measure the current profile; an Optical Backscatter Sensor (OBS-3A, D&A Instrument Company) was used to measure salinity, temperature and turbidity; and an electromagnetic current meter (Alec, Electron-ics, Tokyo) was used to measure the near-bottom current of the bottom zone of the ADCP. The ADCP worked in upward-looking mode to measure the current profile at a vertical resolution of 0.25 m and ensembles of 2 min at a 1-s ping interval. An OBS was dragged along the stern of each boat to measure surface salinity, temperature and turbidity at a sampling rate of 2 min. We calibrated the OBS using water samples, and the calibration process indicated that the instrument worked well.

In addition to the measurement stations in the NB, water level and surface salinity data were collected at the long-term hydrologic stations (red solid circles in Fig. 1) in the SB established by the State Key Laboratory of Estuarine and Coastal Research.

The river discharge at the Datong gauge station was approximately 13,000 m³/s during the observation period (Fig. 2b). This flow rate was slightly higher than the climatological average of 11,800 m³/s in February. Meteorological data were recorded by the weather station located on the Chongming eastern shoal (W, blue solid circles in Fig. 1). The northerly wind and southerly wind alternated during the observation period (Fig. 2c). Moreover, strong wind was detected during the neap tide (February 20, 2017), with a maximum wind speed of 12 m/s.

2.2. Numerical model

A 3D numerical model developed by Wu and Zhu (2010) was used in this study. It was based on the ECOM-si (Blumberg 1994) and later improved by Chen et al. (2001) and Zhu (2003) for studies of hydrodynamics and material transport. The Mellor-Yamada level 2.5 turbulence closure module (Mellor and Yamada 1982) with stability parameters from Kantha and Clayson (1994) was included. Zhu et al. (2002) adopted a predictor-corrector scheme to change the Coriolis terms into a semi-implicit scheme and to improve the model stability in the case of low eddy viscosity. Wu (2006) replaced the fixed boundary in original ECOM-si with a moving boundary to present the process of drying and flooding of tidal flats. Third-order spatial interpolation at a moderate temporal resolution coupled with a TVD limiter (HSIMT-TVD) advection scheme was used in this model to solve the transport equations and prevent numerical oscillations (Wu and Zhu, 2010). This approach has been successfully used in previous studies of saltwater intrusion in the Changjiang Estuary (Wu et al., 2010; Li et al., 2012; Qiu and Zhu, 2013; Qiu and Zhu, 2015). The model used sigma coordinates in the vertical direction and a non-orthogonal curvilinear grid in the horizontal direction. A wet/dry scheme was included to describe the intertidal flat with a critical depth of 0.1 m.

The model domain covered all of the Changjiang Estuary, Hangzhou Bay, and adjacent seas from 117.5°E to 125°E longitude and 27.5°N to 33.7°N latitude (Fig. 3a). The model grid was composed of 337 × 225 cells horizontally and 10 uniform σ levels vertically. The minimum grid resolution was approximately 100 m in the bifurcation of the SB and NB (Fig. 3b) and approximately 200 m in the lower reaches of the NB (Fig. 3c) to effectively simulate SSO. The resolution was decreased to ~10 km at the open boundary. The integrated time step was set to 30 s.

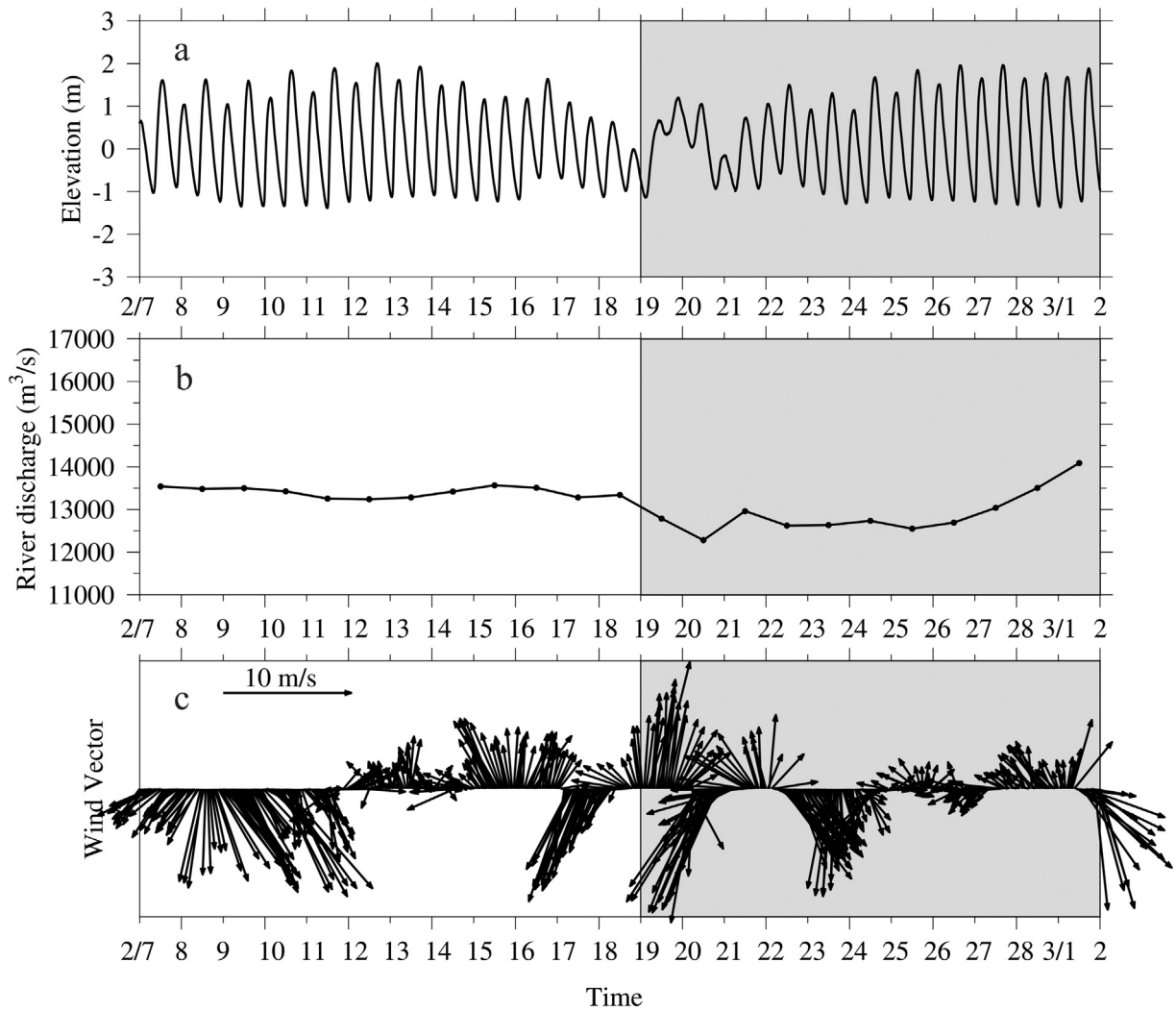


Fig. 2. Temporal variations in the measured water level at Chongxi station (a), river discharge at Datong station (b), and wind vector at the weather station on the Chongming eastern shoal (c) from February 7 to March 1, 2017. The gray area is the observation period.

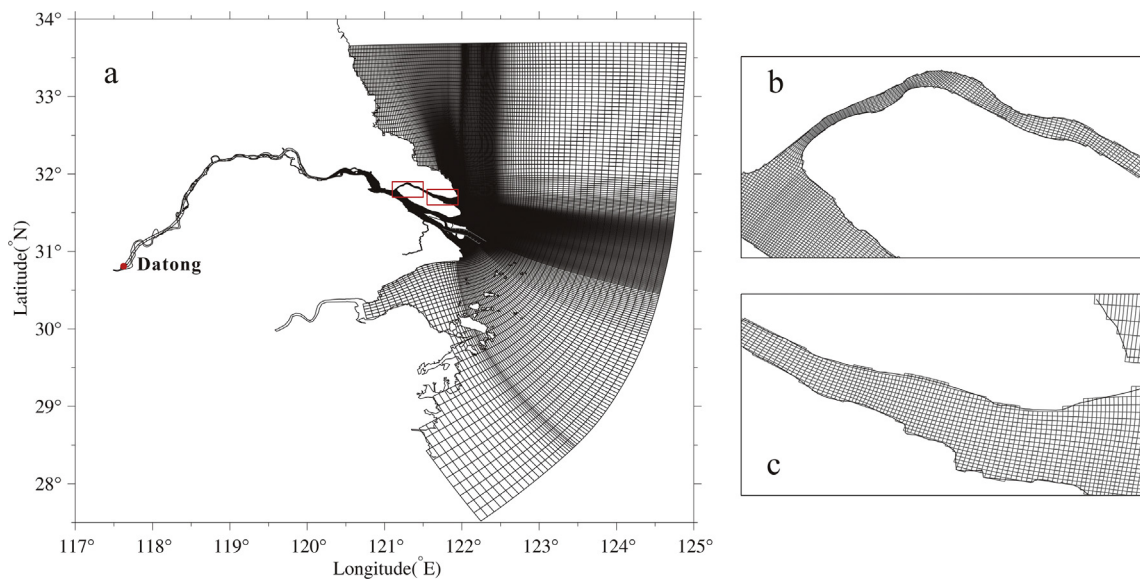


Fig. 3. Model domain (a) and enlarged views of the model grid at the bifurcation between the NB and SB (b) and in the lower reaches of the NB (c).

Derived from the *NaoTide* dataset (<http://www.miz.nao.ac.jp/>), the open sea boundary was driven by 16 astronomical constituents: M_2 , S_2 , N_2 , K_2 , K_1 , O_1 , P_1 , Q_1 , MU_2 , NU_2 , T_2 , L_2 , $2N_2$, J_1 , M_1 , and OO_1 . Daily river discharge recorded at Datong station was used in the model as the river boundary condition. Wind fields, which were used to calculate sea surface momentum, were simulated by the Weather Research Forecast Model (WRF) or using data from the weather station on the Chongming eastern shoal. The National Center for Environmental Prediction (NCEP) reanalysis dataset with a spatial resolution of $0.5^\circ \times 0.5^\circ$ and a temporal resolution of 6 h was used to establish the initial and boundary conditions of the WRF model.

The velocity and elevation were initially set to zero. The initial salinity distribution was derived from the Ocean Atlas of the Huanghai Sea and East China Sea (Hydrology) ([Editorial Board for Marine Atlas, 1992](#)) outside the Changjiang mouth and from recent data collected in the estuary. Because salinity dominates the density variability in the Changjiang Estuary, the water temperature was set to a constant 10°C in the model. Detailed descriptions of the model configuration and validation can be found in [Li et al. \(2012\)](#) and [Qiu and Zhu \(2013\)](#).

2.3. Numerical experiments

We performed two numerical experiments to study the effect of the BDC on saltwater intrusion in the NB. Numerical experiment 1 (Exp1) adopted the logarithmic law of the BDC written as shown in Eq. (2), and numerical experiment 2 (Exp2) used the Chézy-Manning formula given in Eq. (3). Based on previous studies ([Cheng et al., 1993](#); [Bokhorst, 2003](#); [Knight et al., 2009](#)), the Manning roughness coefficient n , as expressed by Eq. (4), was assigned for a range of water depths in the NB. The coefficient varied from 0.010 at water depths greater than 10 m to 0.030 at water depths less than 2.0 m ([Table 1](#)). This method was also used to validate hydrodynamic, salt and heat transport in Ria de Aveiro lagoon ([Dias and Lopes, 2006](#)). Similarly, Ria de Aveiro lagoon is very shallow, and Dias also assigned Manning roughness based on a range of water depths, as did Hilmar [Messal and Mengelkamp \(2006\)](#) when simulating an inundation process in the Ziltendorfer Lowland.

3. Results

3.1. Model validation and evaluation

The numerical model described above has been validated many times in the Changjiang Estuary, and the results suggest that the model can successfully simulate the hydrodynamic processes and saltwater intrusion in the estuary ([Wu et al., 2011](#); [Li et al., 2012](#); [Qiu and Zhu, 2013](#)). In this section, we use the data collected in the NB from February 19 to March 1, 2017, to validate the model for Exp1 and Exp2 and determine which BDC formula better reproduced the hydrodynamic and saltwater intrusion processes.

The following three skill assessment indicators were used to quantify the validation of current and salinity: the correlation coefficient (CC), root-mean-square error (RMSE), and skill score (SS):

Table 1
Manning roughness coefficients in the NB.

Water depth(m)	Value
$D < 2$	0.03
$2 \leq D < 3$	0.024
$3 \leq D < 10$	0.014
$D \geq 10$	0.01

$$CC = \frac{\sum (X_{mod} - \bar{X}_{mod})(X_{obs} - \bar{X}_{obs})}{\left[\sum (X_{mod} - \bar{X}_{mod})^2 \sum (X_{obs} - \bar{X}_{obs})^2 \right]^{1/2}} \quad (5)$$

$$RMSE = \sqrt{\frac{\sum (X_{mod} - X_{obs})^2}{N}} \quad (6)$$

$$SS = 1 - \frac{\sum |X_{mod} - X_{obs}|^2}{\sum (|X_{mod} - \bar{X}_{obs}| + |X_{obs} - \bar{X}_{obs}|)^2} \quad (7)$$

where X_{mod} is the modeled data, X_{obs} is the observed data, and \bar{X} is the mean value. SS is a statistical metric developed by [Willmott \(1981\)](#) to describe the degree to which the observed deviations from the observed mean correspond to the predicted derivations from the observed mean. Perfect agreement between the model results and observations yields an SS of 1.0, whereas complete disagreement yields a value of 0. These metrics were also used by [Warner et al. \(2005\)](#) and [Li et al. \(2005\)](#) to evaluate the consistency between their model results and observations of the Hudson River Estuary and Chesapeake Bay.

Because the NB is extremely shallow, the effect of bottom friction is important, the water velocity of the surface layer is larger than that of the bottom layer, and salinity is almost vertically homogeneous, we choose the water velocities surface and bottom layers and salinities of the surface layers to present their temporal variations. Temporal variations in the observed and modeled water velocities and salinities at stations C, E and G are shown in [Figs. 4–6](#), respectively. The measured data indicated that the water current and salinity exhibited distinct semidiurnal variations. Additionally, the maximum flood velocity was larger than the maximum ebb velocity, and the surface velocity was larger than the bottom velocity. The maximum flood velocities were approximately 2.4, 2.0 and 2.1 m/s in the surface layer and 1.7, 1.5 and 1.6 m/s in the bottom layer at stations C, E and G, respectively. The surface salinities at flood slack were higher than those at ebb slack, and salinity decreased upstream. The maximum values were 7.8, 19.7 and 26.5 at stations C, E and G, respectively. By comparing the modeled and observed data, we can see that the modeled water velocities in Exp2, which is based on the Chézy-Manning BDC formula, were slightly more accurate than those in Exp1, based on a logarithmic BDC formula; however, the modeled salinities improvement in Exp2 exhibited considerable compared to those in Exp1.

The indicator scores of water velocity are summarized in [Table 2](#). In Exp1, the CC at the eight stations ranged from 0.52 to 0.90 in the surface layer, with a mean value of 0.77, and from 0.67 to 0.90 in the bottom layer, with a mean value of 0.77; the RMSE ranged from 0.26 to 0.50 m/s in the surface layer, with a mean value of 0.37 m/s, and from 0.18 to 0.34 m/s in the bottom layer, with a mean value of 0.26 m/s; and the SS ranged from 0.45 to 0.93 in the surface layer, with a mean value of 0.71, and from 0.44 to 0.87 in the bottom layer, with a mean value 0.71.

In Exp2, the CC at the eight measured stations ranged from 0.60 to 0.92 in the surface layer, with a mean value of 0.80, and from 0.65 to 0.90 in the bottom layer, with a mean value of 0.80; the RMSE ranged from 0.24 to 0.49 m/s in the surface layer, with a mean value of 0.35 m/s, and from 0.15 to 0.38 m/s in the bottom layer, with a mean value of 0.26 m/s; and the SS ranged from 0.46 to 0.93 in the surface layer, with a mean value of 0.73, and from 0.42 to 0.92 in the bottom layer, with a mean value of 0.72.

The mean surface and bottom values of CC, RMSE and SS at the eight stations were 0.77, 0.31 m/s and 0.70 in Exp1 and 0.80, 0.30 m/s, and 0.72 in Exp2, respectively. Therefore, the model successfully captured the tidal currents, and the Chézy-Manning formula of BDC provided better results than the logarithmic BDC formula.

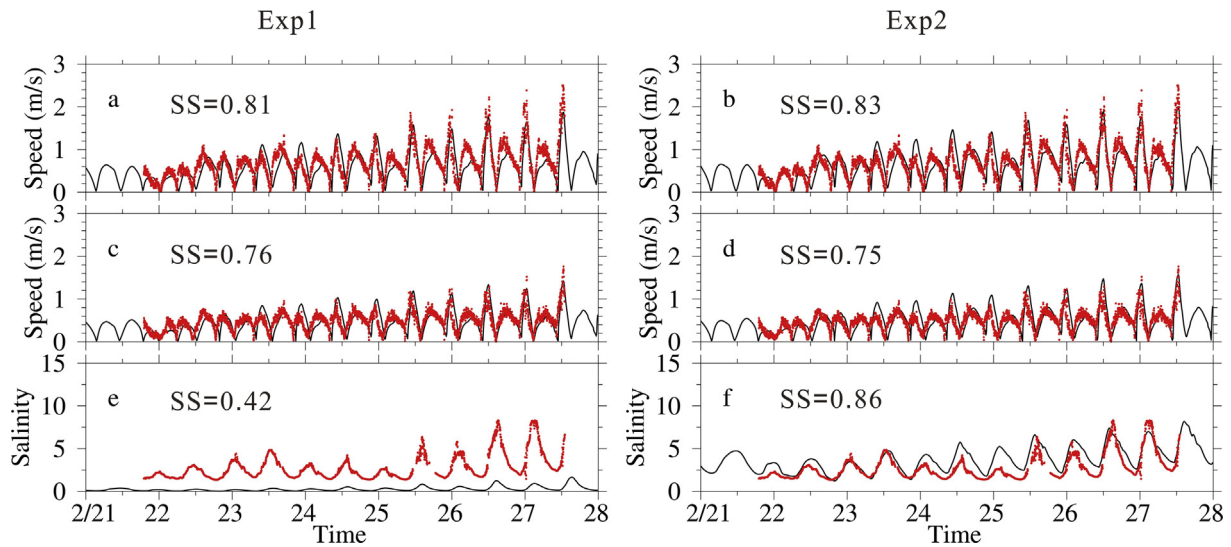


Fig. 4. Comparisons between the modeled data (blank line) and observed data (red dots) at measured station C in Exp1 (left panel) and in Exp2 (right panel). a, b: surface current velocity; c, d: bottom current velocity; e, f: surface salinity. (For interpretation of the references to colour in this figure legend, the reader is referred to the web version of this article.)

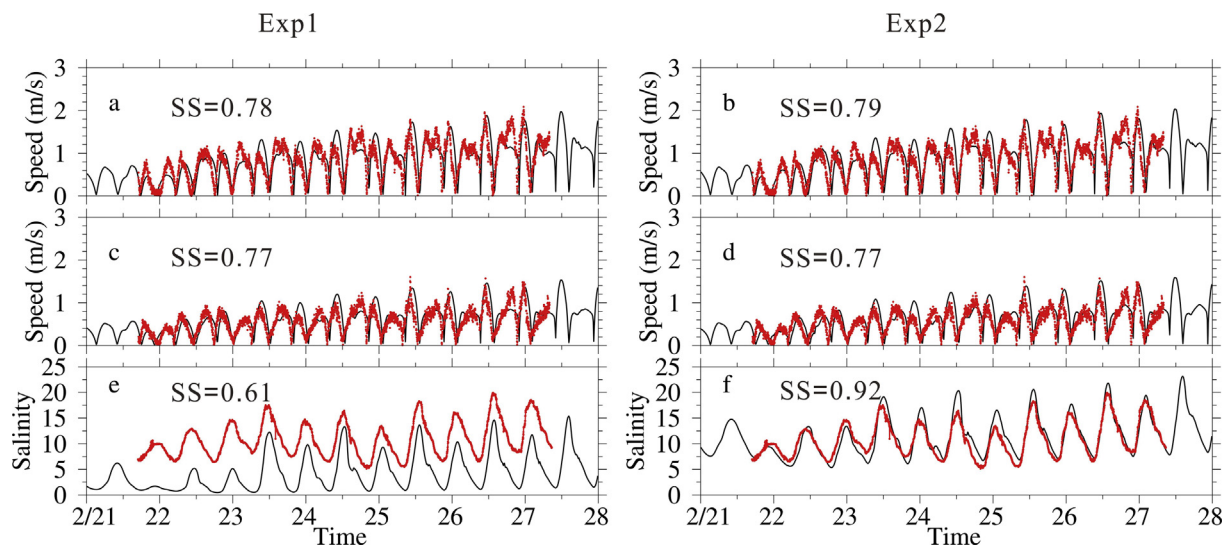


Fig. 5. Comparisons between the modeled data (blank line) and observed data (red dots) at measured station E in Exp1 (left panel) and in Exp2 (right panel). a, b: surface current velocity; c, d: bottom current velocity; e, f: surface salinity. (For interpretation of the references to colour in this figure legend, the reader is referred to the web version of this article.)

The indicator scores of salinity are summarized in Table 3. In Exp1, the CC at the eight stations ranged from 0.64 to 0.93 in the surface layer, with a mean value of 0.83, and from 0.54 to 0.91 in the bottom layer, with a mean value of 0.81; the RMSE ranged from 0.25 to 6.73 in the surface layer, with a mean value of 3.90, and from 0.34 to 8.47 in the bottom layer, with a mean value of 4.64; and the SS ranged from 0.41 to 0.77 in the surface layer, with a mean value of 0.52, and from 0.22 to 0.70 in the bottom layer, with a mean value of 0.47.

In Exp2, the CC at the eight stations ranged from 0.79 to 0.92 in the surface layer, with a mean value of 0.87 at surface layer, and from 0.65 to 0.92 in the bottom layer, with a mean value of 0.84; the RMSE ranged from 0.13 to 3.54 in the surface layer, with a mean value of 1.79, and from 0.23 to 3.29 in the bottom layer, with a mean value of 1.86; and the SS ranged from 0.65 to 0.92 in the surface layer, with a mean value of 0.84, and from 0.43 to 0.95 in the bottom layer, with a mean value of 0.79.

The mean surface and bottom values of CC, RMSE and SS of salinity at the eight stations were 0.82, 4.27 and 0.49 in Exp1 and 0.85, 1.82 and 0.82 in Exp2, respectively. The SS was significantly higher in Exp2 than in Exp1, indicating that the model based on the logarithmic BDC formula underestimated salinity in the NB, and the model based on the Chézy-Manning formula of BDC successfully captured the temporal variations in salinity in the NB.

3.2. Mechanisms and discussion

To improve the representativeness of the study, we used the mean river discharge and wind in winter to simulate climatological saltwater intrusion in Exp1 and Exp2 and study the effects of different drag coefficients on saltwater intrusion. The river discharge was set to 11,800 m³/s, which was the climatological mean in January and February from 1950 to 2015. The surface

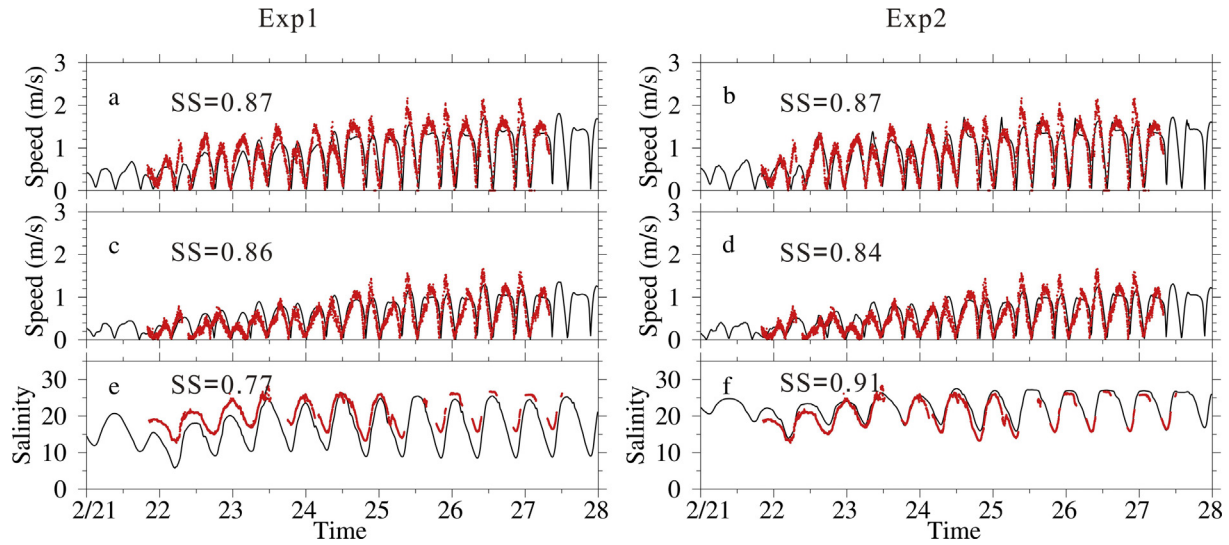


Fig. 6. Comparisons between the modeled data (blank line) and observed data (red dots) at measured station G in Exp1 (left panel) and in Exp2 (right panel). a, b: surface current velocity; c, d: bottom current velocity; e, f: surface salinity. (For interpretation of the references to colour in this figure legend, the reader is referred to the web version of this article.)

Table 2
Correlation coefficients (CC), root-mean-square error (RMSE), and skill scores (SS) for comparison of Modeled and observed water velocity at the measured stations (value at surface layer/value at bottom layer).

Station	Exp1			Exp2		
	CC	RMSE	SS	CC	RMSE	SS
A	0.64/0.67	0.48/0.34	0.45/0.44	0.67/0.65	0.46/0.37	0.46/0.42
B	0.84/0.79	0.50/0.34	0.54/0.51	0.83/0.78	0.49/0.38	0.57/0.48
C	0.78/0.74	0.32/0.23	0.81/0.76	0.81/0.75	0.30/0.24	0.83/0.75
D	0.89/0.87	0.39/0.21	0.87/0.91	0.90/0.88	0.35/0.21	0.89/0.91
E	0.76/0.74	0.36/0.27	0.78/0.77	0.77/0.76	0.36/0.28	0.79/0.77
F	0.90/0.90	0.33/0.22	0.93/0.93	0.92/0.90	0.30/0.23	0.93/0.92
G	0.84/0.83	0.31/0.24	0.87/0.86	0.83/0.81	0.34/0.26	0.87/0.84
H	0.52/0.67	0.26/0.18	0.47/0.49	0.60/0.76	0.24/0.15	0.51/0.64

Table 3
Correlation coefficients (CC), root-mean-square error (RMSE), and skill scores (SS) for comparison of Modeled and observed salinity at the measured stations (value at surface layer/value at bottom layer).

Station	Exp1			Exp2		
	CC	RMSE	SS	CC	RMSE	SS
A	0.78/0.69	0.25/0.34	0.41/0.22	0.84/0.77	0.13/0.23	0.80/0.43
B	0.80/0.84	1.66/2.10	0.41/0.43	0.84/0.87	0.52/0.62	0.89/0.90
C	0.92/0.91	2.80/3.16	0.42/0.42	0.88/0.90	1.10/1.02	0.86/0.90
D	0.85/0.87	6.51/7.68	0.49/0.49	0.88/0.89	2.08/2.27	0.89/0.90
E	0.90/0.91	5.82/6.85	0.61/0.59	0.92/0.92	2.01/1.82	0.92/0.95
F	0.85/0.87	6.73/8.47	0.64/0.55	0.85/0.87	3.54/2.72	0.83/0.88
G	0.93/0.87	4.95/6.37	0.77/0.70	0.91/0.86	2.26/2.91	0.91/0.86
H	0.64/0.54	2.47/2.14	0.43/0.35	0.79/0.65	2.68/3.29	0.65/0.53

wind was set to a constant northerly direction and speed of 5 m/s, which are approximately the mean wind conditions in winter.

3.2.1. BDC

The logarithmic formula of BDC is closely related to z_b (see formula (2)), which is the height of half the bottom layer from the bottom of the model. Each vertical layer thickness varies with the total water depth. The BDC will decrease when the total water depth increases during flood tide. Inserting formula (4) into formula (3), the BDC of the Chézy-Manning formula can be written as follows.

$$C_d = \frac{gn^2}{\sqrt[3]{H}} \quad (8)$$

Therefore, the BDC is related to water depth and the Manning roughness coefficient n . C_d will increase when the water depth decreases. The Manning roughness coefficient n is dependent on water depth H (Table 1) and increases with decreasing H . Overall, C_d increases as H decreases. The NB is extremely shallow, and the tidal range is large (Zhu et al., 2015); therefore, the total water depth varies significantly with the flood and ebb tides.

To show the variation in the BDC with the tide, we calculated the BDC distribution in Exp1 and in Exp2 during spring tide at

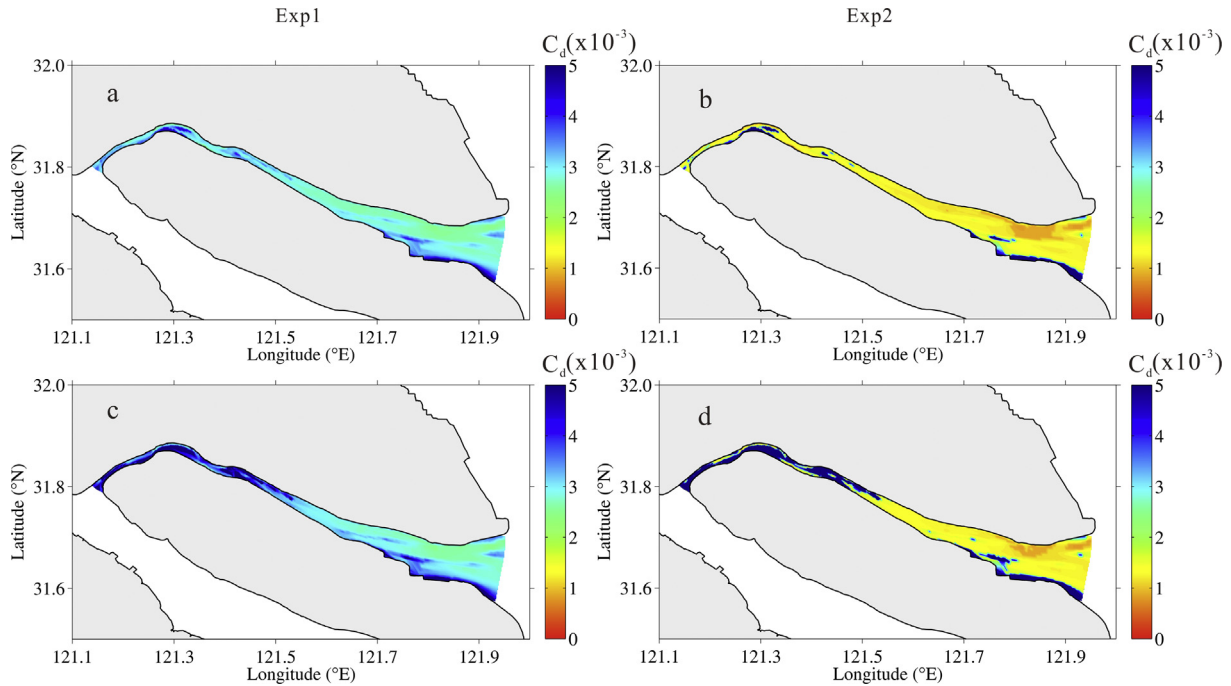


Fig. 7. Distribution of the BDC in Exp1 (left panel) and Exp2 (right panel) during spring tide. a, b: at the highest tidal level; c, d: at the lowest tidal level. The reference site of the highest and lowest tidal levels is measurement station D.

the highest and lowest tidal levels (Fig. 7). In Exp1, the BDC is approximately 2.5×10^{-3} in most areas of the NB and approximately 3.5×10^{-3} in some very shallow areas at the highest tidal level (Fig. 7a). At the lowest tidal level, when the NB becomes extremely shallow, the BDC is approximately 4.1×10^{-3} in most areas of the upper and middle reaches of the NB and is slightly larger in the lower reaches of the NB compared with that at the highest tidal level (Fig. 7c). In Exp2, the BDC is approximately 1.5×10^{-3} in most areas of the NB and approximately 3.2×10^{-3} in some very shallow areas at the highest tidal level (Fig. 7b). At the lowest tidal level, the BDC is approximately 4.3×10^{-3} in most areas of the upper and middle reaches of the NB and is slightly larger in the lower reaches of the NB compared with that at the highest tidal level (Fig. 7d). Therefore, the BDC increases according to both the logarithmic and Chézy-Manning formulas when the water depth decreases, and the BDC values produced by the Chézy-Manning formula are smaller than those of the logarithmic formula. This difference could influence estimates of the net water flux and saltwater intrusion in the NB, especially in the upper reaches of the NB.

3.2.2. Net water flux per unit width

To describe the subtidal movements of water in the Changjiang Estuary, we defined the instantaneous rate of water transport per unit width through a water column as follows.

$$\vec{Q} = \int_{-1}^0 H \vec{V} d\sigma \quad (9)$$

Then, the residual (net) transport of water (\vec{Rw}) per unit width was calculated as follows.

$$\vec{Rw} = \frac{1}{T} \int_0^T \vec{Q} dt \quad (10)$$

where H is the total water depth, \vec{V} is the current velocity vector, σ is the relative depth (0 at the surface and -1 at the bottom), and T is the time period (which equals one or several tidal cycles). In this

study, six semidiurnal tidal cycles, or ~ 3 d, were used as an averaging time window to remove the semidiurnal and diurnal tidal signals.

In Exp1, during spring tide, the residual water flux per unit width in the NB flows landward on the south side and seaward on the north side of the middle and lower reaches (Fig. 8a). During neap tide, the flux is smaller and flows seaward in the entire NB (Fig. 8c). In Exp2, during spring tide, the residual water flux per unit width still flows upstream, but its magnitude is larger in the upper reaches than that in Exp1. Additionally, the magnitude of the landward net water flux is largest in the lower reaches on the south side of the NB (Fig. 8c). During neap tide, the net water flux is nearly equal to that in Exp1 (Fig. 8d). The landward net water flux in the upper reaches of the NB during spring tide is evidently larger based on the Chézy-Manning formula of the BDC than that based on the logarithmic BDC formula because the bottom friction in the former equation is much smaller than that in the latter equation.

3.2.3. Saltwater intrusion

In Exp1, during spring tide, the NB is filled with highly saline water, and the isohaline of 5 is close to the bifurcation of the NB and SB at the flood slack. Only a small area of salinity greater than 1 appears in the upper reaches of the SB, suggesting that SSO is weak during the spring tide (Fig. 9a). During neap tide, the salinity in the upper reaches of the NB decreases at the flood slack, and no SSO occurs (Fig. 9c). In Exp2, the isohalines in the upper reaches of the NB move upstream compared to those in Exp1, indicating that saltwater intrusion becomes stronger (Fig. 9b). Moreover, the area of salinity greater than 1 in the SB distinctly increases, suggesting that SSO occurs. During neap tide, only a small area of salinity greater than 1 in the SB exists along the south coast of Chongming Island, and SSO ceases (Fig. 9d). Estimates of saltwater intrusion in the NB were enhanced using the logarithmic BDC formula compared to using the Chézy-Manning formula of BDC, especially in the upper reaches of the NB. This finding is consistent with the dynamic variation in the net water flux discussed above.

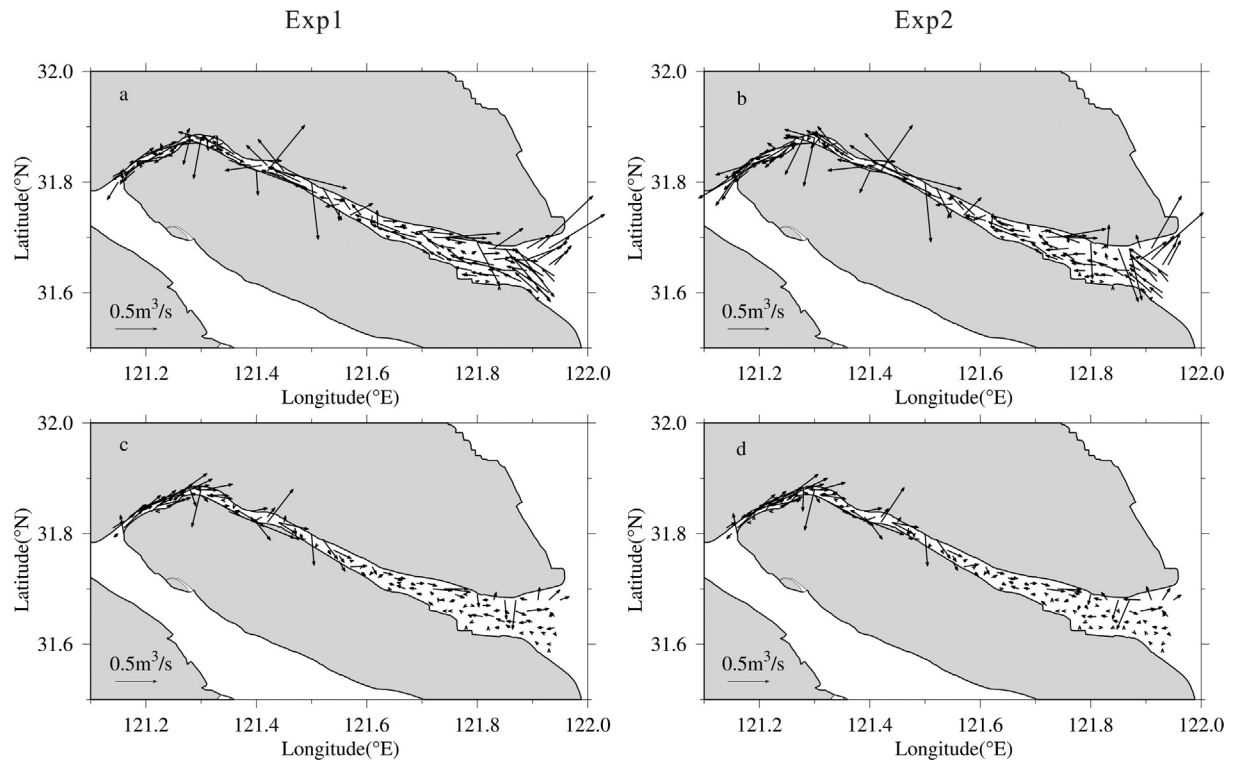


Fig. 8. Distribution of unit width residual water flux in the NB in Exp1 (left panel) and in Exp2 (right panel). a, b: during spring tide; c, d: during neap tide.

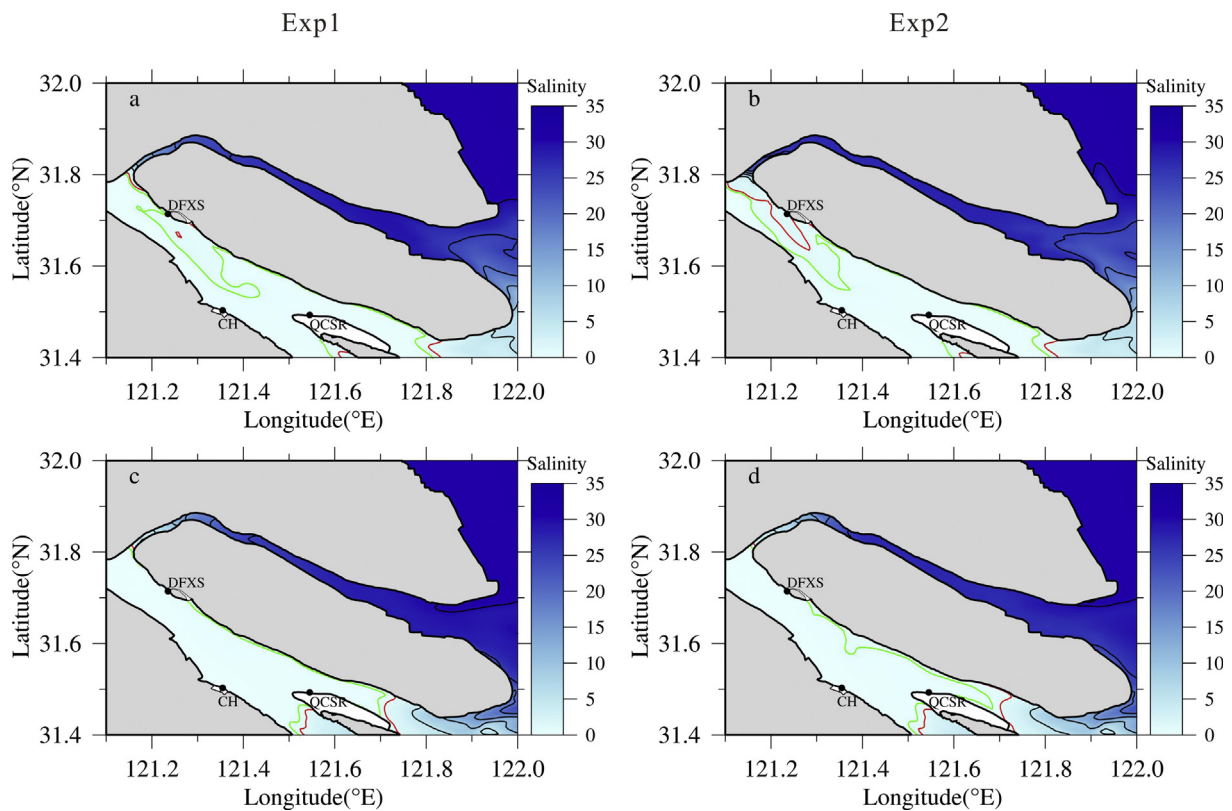


Fig. 9. Distribution of depth-averaged salinity at flood slack in Exp1 (left panel) and in Exp2 (right panel). a, b: during spring tide; c, d: during neap tide. The green isohaline is 0.45, red isohaline is 1, black isohalines begins 5 with interval 5. (For interpretation of the references to colour in this figure legend, the reader is referred to the web version of this article.)

3.2.4. SSO

The most characteristic form of saltwater intrusion in the Changjiang Estuary is SSO, which is closely related to the saltwater intrusion in the NB. We established a transect sec1 in the upper reaches of the NB near the bifurcation (labeled in Fig. 1) to study the effect of the BDC on the water and salt fluxes through the transect. The net transect water flux (NTWF) and net transect salt flux (NTSF) were calculated as follows.

$$NTWF = \frac{1}{T} \int_0^T \int_{-H(x,y)}^{\zeta} \int_0^L \vec{V}_n(x,y,z,t) dldzdt \quad (11)$$

$$NTSF = \frac{1}{T} \int_0^T \int_{-H(x,y)}^{\zeta} \int_0^L s \vec{V}_n(x,y,z,t) dldzdt \quad (12)$$

where ζ is the surface elevation, L is the width of the transect, s is the salinity, and $\vec{V}_n(x,y,z,t)$ is the velocity component normal to the transect.

As shown in Table 4, the NTWF is upstream in spring tide and downstream in neap tide in Exp1 and Exp2, but the values are much larger in Exp2 than in Exp1, with differences of -251.68 and $44.77 \text{ m}^3/\text{s}$, respectively. This result suggests that more water is transported from the NB into the SB during spring tide and more water is transported from the SB into the NB during neap tide. The NTSF varied similarly to the NTWF, but the NTSF in Exp2 was approximately 1.8 times higher than the value in Exp1 during spring tide, indicating that SSO was 1.8 times higher based on the Chézy-Manning formula of BDC than based on the logarithmic BDC formula. In neap tide, the NTSF is from the NB into the SB in Exp1 but from the SB into the NB in Exp2, and the flux is much smaller than that during spring tide. The quantitative relationship of runoff and tidal range to the intensity of SSO obtained by Wu et al. (2006) for the first time, which indicates that the SSO

increases exponentially with the increase of tidal range, and declines exponentially with the increase of runoff. Our model results are consistent with the conclusion of Wu et al.

After saltwater enters the SB via SSO, it moves downstream under the force of runoff and influences the downstream salinity at the hydrological stations. The Chongxi and Nanmen hydrological stations (labeled in Fig. 1) are located on the southwest coast of Chongming Island, and salinity there is completely due to SSO (Wu et al., 2006; Li et al. 2012). The salinities at the two hydrological stations are distinctly higher in Exp2 than in Exp1 (Fig. 10). At Chongxi hydrological station, only sharp pulses of salinity exceed the salinity standard of drinking water in Exp1, but salinity is higher than 0.45 more than half of the time in February in Exp2. At Nanmen hydrological station, the salinity is slightly higher than 0.45 in some short periods and nearly lower than 0.45 in all of February in Exp1, but the salinity is higher than 0.45 for approximately half of February in Exp2. Therefore, adopting the Chézy-Manning formula rather than the logarithmic BDC formula can overcome the issue of underestimating SSO noted in previous studies.

As stated above, we analyzed the SSO based on the climatological states of river discharge and wind in winter, but SSO can be greatly enhanced when a cold front passes over the Changjiang Estuary (Li et al., 2012). Strong northerly winds could induce landward Ekman water transport and strengthen SSO. Next, we present how SSO responded to a strong northerly wind event from March 8 to 10, 2016, with different BDC formulas. The river discharge measured at Datong station ranged from 16,000 to 21,000 m^3/s , with a mean value of 18,000 m^3/s , from March 1 to 15, 2016 (Fig. 11a). Under normal circumstances, SSO would weaken when river discharge reaches 18,000 m^3/s . A strong northerly wind affected the estuary from March 8 to 10, 2016, with a maximum wind speed of 23 m/s and mean wind speed of 13 m/s (Fig. 11b). The highest tidal level was predicted to occur on March 11, 2016 (the third day of the lunar calendar), but was observed on March 9, 2016, due to the strong northerly wind during the medium tide after neap tide (Fig. 11c).

The strong northerly wind induced SSO in the case of high river discharge, and this influence was record at Chongxi and Nanmen hydrological stations (Fig. 12). The results of the numerical model indicate that the model successfully hindcast SSO and the temporal variations in salinity at the two hydrological stations using the Chézy-Manning formula of BDC but underestimated the salinity when the logarithmic BDC formula was used. Therefore, we further

Table 4
The NTWF and NTSF through sect1 in Exp1 and Exp2 (a minus sign indicates a flux from the NB to the SB, and a plus sign indicates a flux in the opposite direction).

	NTWF(m^3/s)		NTSF(t/s)	
	Spring	Neap	Spring	Neap
Exp1	-210.54	71.99	-6.09	-0.34
Exp2	-462.22	116.76	-11.18	0.23
$\Delta_{\text{Exp2-Exp1}}$	-251.68	44.77	-5.09	0.57

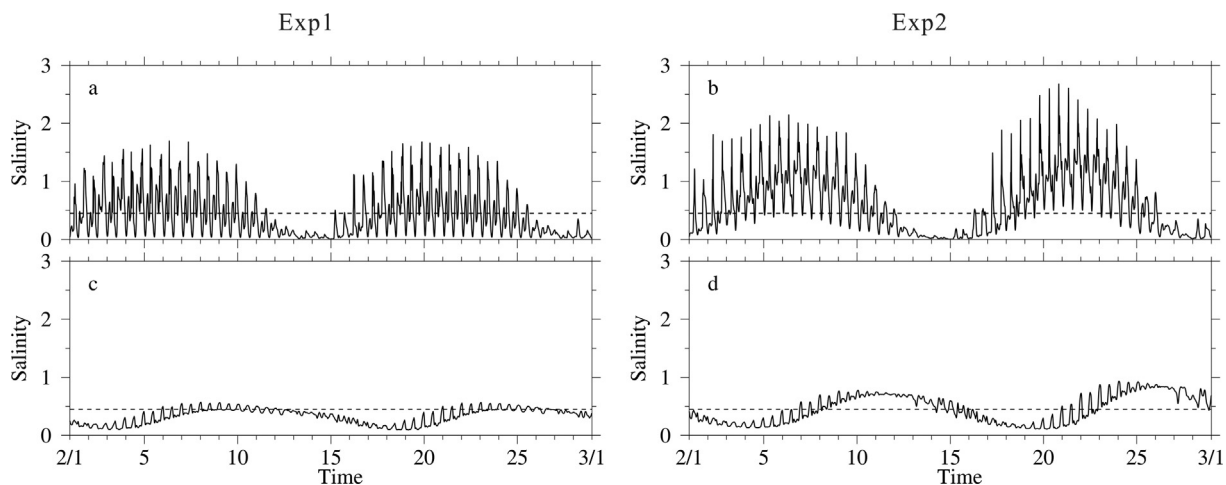


Fig. 10. Temporal variations in salinity in Exp1 (left panel) and Exp2 (right panel). a, b: at Chongxi hydrological station; c, d: at Nanmen hydrological station. The dashed line is a salinity of 0.45, which is the standard of drinking water.

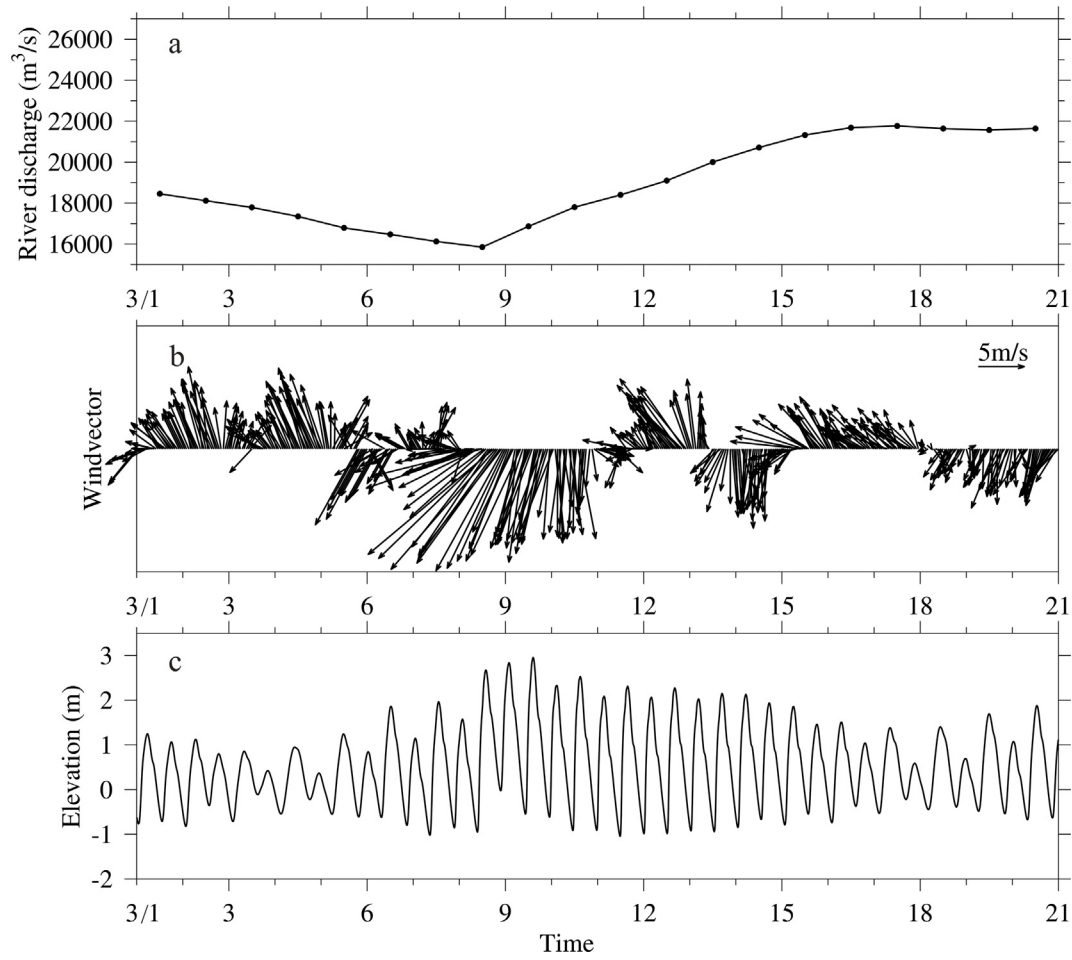


Fig. 11. Temporal variations of the measured river discharge at Datong station (a), wind vector at weather station at Chongming eastern shoal (b), water level at Chongxi hydrological station (c) during March 1 to 20, 2016.

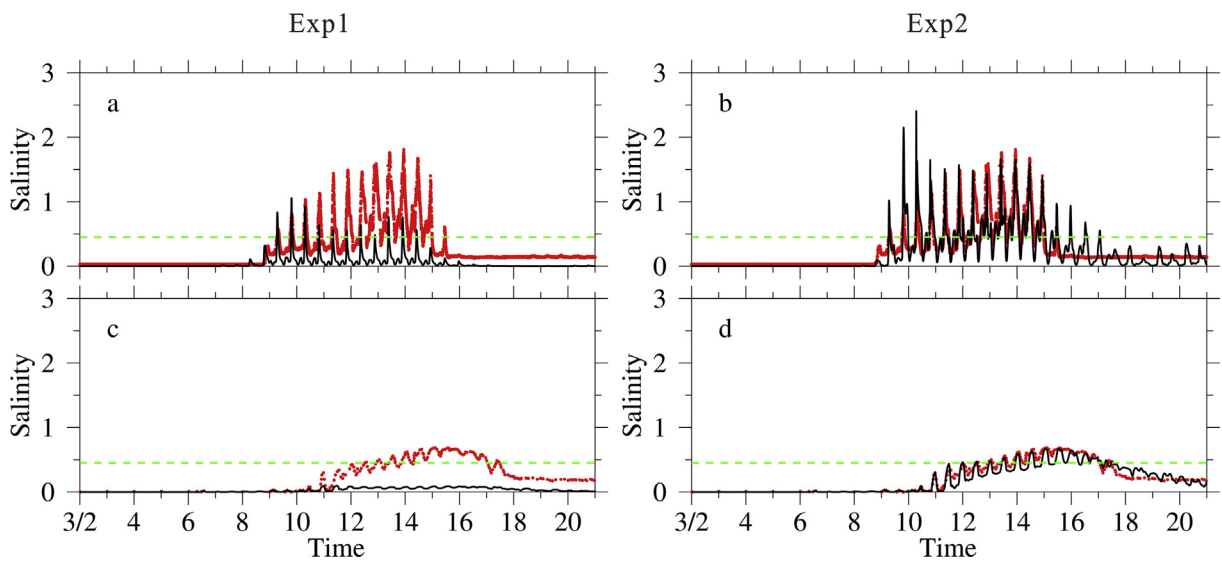


Fig. 12. Temporal variation of salinity in Exp1 (left panel) and in Exp2 (right panel) during March 2 to 20, 2016. a, b: at Chongxi hydrological station; c, d: at Nanmen hydrological station. The black line denotes modeled data and red dots denote measured data. The green dashed line is salinity 0.45, the standard of drink water. (For interpretation of the references to colour in this figure legend, the reader is referred to the web version of this article.)

confirm that the BDC has an important influence on the SSO in the estuary. Approximately 80% of freshwater in Shanghai is currently taken from the reservoirs in the Changjiang Estuary, and the most severe challenge is saltwater intrusion in winter, especially SSO. It is important to adopt a suitable BDC to ensure water safety in the megalopolis of Shanghai and improve the numerical forecasting accuracy of saltwater intrusion in the estuary.

4. Conclusions

The NB is extremely shallow, and the upper reaches of the NB are almost orthogonal to the SB. Additionally, the lower reaches of the NB are funnel shaped. The river regime of the NB helps prevent runoff from entering the NB during the dry season and makes the tidal range larger in the NB than in the SB. The interaction between the topography and dynamic processes in the NB produces a special type of saltwater intrusion, SSO, which threatens the winter water supplies of the reservoirs located in the estuary. The improved ECOM-si model with the advection scheme HSIMT-TVD was applied in this study. Logarithmic and Chézy-Manning BDC formulas were established in the model to investigate the associated effects on saltwater intrusion in the NB. The Manning roughness coefficient was assigned based on a range of water depths and varied from 0.010 at water depths greater than 10 m to 0.030 at water depths less than 2.0 m.

A comparison of the results between the modeled data and data collected at the eight measurement stations in the NB from February 19 to March 1, 2017, showed that the water velocities modeled using the Chézy-Manning formula of BDC were slightly more accurate than those based on the logarithmic BDC formula; however, the salinities modeled using the Chézy-Manning formula were more accurate than those of the logarithmic formula. Three skill assessment indicators, CC, RMSE and SS, were used to quantify the model validation of the water velocity and salinity. For the logarithmic BDC formula, the values of CC, RMSE and SS were 0.77, 0.31 m/s and 0.70 for water velocity and 0.82, 4.27 and 0.49 for salinity, respectively. The model simulated the tidal currents fairly well but distinctly underestimated the salinity in the NB. For the Chézy-Manning formula of BDC, the values of CC, RMSE and SS were 0.80, 0.30 m/s, and 0.72 for water velocity and 0.85, 1.82 and 0.82 for salinity, respectively. The model successfully captured the tidal currents and salinity in the NB, and outperformed the logarithmic BDC formula, especially in salinity estimation.

The BDC increases when water depth decreases during ebb tide and is notably smaller in the upper reaches of the NB at the highest tidal level of spring tide based on the Chézy-Manning formula versus the logarithmic formula. During spring tide, the residual water flux per unit width in the NB flows landward on the south side and seaward on the north side of the middle and lower reaches, and the flow is landward in the upper reaches of the NB. During neap tide, the flux is smaller than that during spring tide and flows seaward in the entire NB. A comparison of the results based on the Chézy-Manning BDC formula and those based on the logarithmic BDC formula showed that the landward net water flux in the upper reaches of the NB considerably increases during spring tide. Additionally, saltwater intrusion in the NB increases at this time, especially in the upper reaches of the NB. This finding is consistent with the dynamic changes in the net water flux. At the transect in the upper reaches of the NB, the NTWF is upstream in spring tide and downstream in neap tide. Moreover, SSO was 1.8 times larger in Exp2 than in Exp1 during spring tide. In neap tide, the NTSF is from the NB into the SB based on the logarithmic BDC formula but from the SB into the NB based on the Chézy-Manning formula, and the flux is much smaller compared to that during spring tide.

SSO varies based on the climatological states of river discharge and wind in winter. For example, high river discharge and a strong northerly wind caused the model to underestimate SSO and salinity at the hydrological stations in the SB based on the logarithmic BDC formula; however, SSO and temporal variations in salinity in the SB were successfully modeled using the Chézy-Manning formula of BDC. The BDC has an important effect on SSO. Notably, it is important to adopt a suitable BDC to ensure water safety in the megalopolis of Shanghai and improve the numerical forecasting accuracy of saltwater intrusion in the estuary.

Acknowledgements

This work was supported by the National Natural Science Foundation of China (41476077, 41676083). We also acknowledge the anonymous reviewers for their valuable comments and suggestions.

References

- Batchelor, G.K., 1953. Book reviews: the theory of homogeneous turbulence. *Math. Gazette* 118. <https://doi.org/10.1126/science.118.3056.118-a>.
- Blumberg, A.F., 1994. A primer for ECOM-si. Technical report of HydroQual, 66.
- Bokhorst, J.S., 2003. A new wind-formulation for hydrodynamic models. Tu Delft Faculty of Civil Engineering & Geosciences Hydraulic Engineering.
- Cameron, W.M., Prichard, D.W., 1963. Estuaries. In: Hill, M. (Ed.), *The sea*, vol. 2. John Wiley & Sons, New York, pp. 306–324.
- Chen, C., Zhu, J., Ralph, E., Green, S.A., Budd, J.W., Zhang, F.Y., 2001. Prognostic modeling studies of the Keweenaw current in Lake Superior. Part I: Formation and evolution. *J. Phys. Oceanogr.* 31 (2), 379–395. [https://doi.org/10.1175/1520-0485\(2001\)031<0379:PMSOTK>2.0.CO;2](https://doi.org/10.1175/1520-0485(2001)031<0379:PMSOTK>2.0.CO;2).
- Cheng, R.T., Casulli, V., Gartner, J.W., 1993. Tidal, Residual, Intertidal Mudflat (TRIM) Model and its Applications to San Francisco Bay, California. *Estuarine Coastal Shelf Sci.* 36 (3), 235–280. <https://doi.org/10.1006/ecss.1993.1016>.
- Chow, V.T., 1959. *Open-Channel Hydraulics*. Open-channel hydraulics. McGraw-Hill.
- Collins, M.B., Ke, X., Gao, S., 1998. Tidally-induced flow structure over intertidal flats. *Estuar. Coast. Shelf Sci.* 46 (2), 233–250. <https://doi.org/10.1006/ecss.1997.0260>.
- Dias, J.M., Lopes, J.F., 2006. Calibration and validation of hydrodynamic, salt and heat transport models for Ria de Aveiro Lagoon (Portugal). *J. Coast. Res.* S13 39, 1680–1684. <http://www.jstor.org/stable/25743045>.
- Dronkers, J.J., 1964. Tidal computations in rivers and coastal waters. Tidal computations in rivers and coastal waters. North-Holland Pub. Co.
- Dunbar, D., Leblond, P., Murty, T.S., 1991. Evaluation of tsunami amplitudes for the Pacific Coast of Canada. *Prog. Oceanogr.* 26 (26), 115–177. [https://doi.org/10.1016/0079-6611\(91\)90001-3](https://doi.org/10.1016/0079-6611(91)90001-3).
- Dyer, K.R., 1980. Velocity profiles over a rippled bed and the threshold of movement of sand. *Estuar. Coast. Mar. Sci.* 10 (2), 181–199. [https://doi.org/10.1016/S0302-3524\(80\)80057-0](https://doi.org/10.1016/S0302-3524(80)80057-0).
- Editorial Board for Marine Atlas, 1992. *Ocean Atlas in Huanghai Sea and East China Sea (Hydrology)*. China Ocean Press, Beijing.
- Geyer, W.R., 1993. The importance of suppression of turbulence by stratification on the estuarine turbidity maximum. *Estuaries Coasts* 16 (1), 113–125. <https://doi.org/10.2307/1352769>.
- Gong, W.P., Shen, J., 2011. The response of salt intrusion to changes in river discharge and tidal mixing during the dry season in the Modaomen Estuary, China. *Continental Shelf Res.* 31 (7–8), 769–788. <https://doi.org/10.1016/j.csr.2011.01.011>.
- Messal, H., Mengelkamp, H.T., 2006. Inundation of the Ziltendorfer Lowland during the Odra flood 1997 and its impact on the main river - a numerical study. *J. Hydroinf.* 8 (3), 181–192.
- Kantha, L.H., Clayson, C.A., 1994. An improved mixed layer model for geophysical applications. *J. Geophys. Res. Oceans* 99 (C12), 25235–25266. <https://doi.org/10.1029/94JC02257>.
- Knight, D.W., 1981. Some field measurements concerned with the behaviour of resistance coefficients in a tidal channel. *Estuar. Coast. Shelf Sci.* 12 (3), 303–322. [https://doi.org/10.1016/S0302-3524\(81\)80127-2](https://doi.org/10.1016/S0302-3524(81)80127-2).
- Knight, D.W., Caroline, M.G., Rob, L., Paul, G.S., 2009. *Practical Channel Hydraulics: Roughness, Conveyance and Afflux*.
- Li, L., Zhu, J.R., Wu, H., 2012. Impacts of wind stress on saltwater intrusion in the Yangtze Estuary. *Science China Earth Sciences* 55 (7), 1178–1192. <https://doi.org/10.1007/s11430-011-4311-1>.
- Li, L., Zhu, J.R., Wu, H., Guo, Z.G., 2014. Lateral saltwater intrusion in the North Channel of the Changjiang Estuary. *Estuaries Coasts* 37 (1), 36–55. <https://doi.org/10.1007/s12237-013-9669-1>.
- Li, L., Zhu, J.R., Wu, H., Wang, B., 2010. A numerical study on water diversion ratio of the Changjiang (Yangtze) estuary in dry season. *Chin. J. Oceanol. Limnol.* 28 (3), 700–712. <https://doi.org/10.1007/s00343-010-9114-2>.

- Li, M., Zhong, L., Boicourt, W.C., 2005. Simulations of Chesapeake Bay estuary: Sensitivity to turbulence mixing parameterizations and comparison with observations. *J. Geophys. Res. Oceans* 110 (C12), 347–356. <https://doi.org/10.1029/2004JC002585>.
- Ludwick, J.C., 1975. Variations in the boundary-drag coefficient in the tidal entrance to Chesapeake Bay, Virginia. *Marine Geol.* 19 (1), 19–28. [https://doi.org/10.1016/0025-3227\(75\)90003-1](https://doi.org/10.1016/0025-3227(75)90003-1).
- Lueck, R.G., 1988. Turbulent mixing at the Pacific subtropical front. *J. Phys. Oceanogr.* 18 (12), 1761–1774. [https://doi.org/10.1175/1520-0485\(1988\)018<1761:TMATPS>2.0.CO;2](https://doi.org/10.1175/1520-0485(1988)018<1761:TMATPS>2.0.CO;2).
- Mellor, G.L., Yamada, T., 1982. Development of a turbulence closure model for geophysical fluid problems. *Rev. Geophys.* 20 (4), 851–875. <https://doi.org/10.1029/RC020i004p00851>.
- Prichard, D.W., 1955. Estuarine circulation patterns. *Proc. Amer. Civil Eng.* 81 (717).
- Pritchard, D.W., 1956. The dynamic structure of a coastal plain estuary. *J. Marine Res.*, 33–42.
- Qian, N., Hong, R.J., Mai, Q.W., Bi, C.F., 1959. Channel roughness of lower Yellow River. *J. Sediment Res.* [in Chinese with English abstract]
- Qiu, C., Zhu, J.R., 2013. Influence of seasonal runoff regulation by the Three Gorges Reservoir on saltwater intrusion in the Changjiang River Estuary. *Cont. Shelf Res.* 71, 16–26. <https://doi.org/10.1016/j.csr.2013.09.024>.
- Qiu, C., Zhu, J.R., 2015. Assessing the influence of sea level rise on salt transport processes and estuarine circulation in the Changjiang River estuary. *J. Coastal Res.* 31 (3), 661–670 <http://www.bioone.org/doi/abs/10.2112/JCOASTRES-D-13-00138.1>.
- Qiu, C., Zhu, J.R., Gu, Y.L., 2012. Impact of seasonal tide variation on saltwater intrusion in the Changjiang River estuary. *Chin. J. Oceanol. Limnol.* 30 (2), 342–351. <https://doi.org/10.1007/s00343-012-1115-x>.
- Ree, W.O., 1981. Flow of water in channels protected by vegetative linings. *Technical Bulletins.*
- Shen, H.T., Mao, Z.C., Zhu, J.R., 2003. Saltwater intrusion in the Changjiang Estuary. Beijing: China Ocean, 175p [in Chinese with English abstract].
- Simpson, J.H., Brown, J., Matthews, J., Allen, G., 1990. Tidal straining, density currents, and stirring in the control of estuarine stratification. *Estuaries Coasts* 13 (2), 125–132. <https://doi.org/10.2307/1351581>.
- Soulsby, R.L., Dyer, K.R., 1981. The form of the near-bed velocity profile in a tidally accelerating flow. *J. Geophys. Res. Oceans* 86 (C9), 8067–8074. <https://doi.org/10.1029/JC086iC09p08067>.
- Wang, B., Zhu, J.R., Hui, W., Yu, F.J., Song, X.J., 2012. Dynamics of saltwater intrusion in the Modaomen Waterway of the Pearl River Estuary. *Science China Earth Sciences* 55 (11), 1901–1918. <https://doi.org/10.1007/s11430-012-4371-x>.
- Warner, J.C., Geyer, W.R., Lerczak, J.A., 2005. Numerical modeling of an estuary: a comprehensive skill assessment. *J. Geophys. Res. Oceans* 110 (5), 297–314. <https://doi.org/10.1029/2004JC002691>.
- Willmott, C.J., 1981. On the validation of models. *Phys. Geography* 2 (2), 184–194. <https://doi.org/10.1080/02723646.1981.10642213>.
- Wu, H., 2006. Saltwater intrusion in the Changjiang Estuary. *East China Normal University*, 19–20 [in Chinese with English abstract].
- Wu, H., Zhu, J.R., 2010. Advection scheme with 3rd high-order spatial interpolation at the middle temporal level and its application to saltwater intrusion in the Changjiang Estuary. *Ocean Model.* 33 (1), 33–51. <https://doi.org/10.1016/j.ocemod.2009.12.001>.
- Wu, H., Zhu, J.R., Chen, B.R., Chen, Y.Z., 2006. Quantitative relationship of runoff and tide to saltwater spilling over from the North Branch in the Changjiang Estuary: a numerical study. *Estuar. Coast. Shelf Sci.* 69 (1–2), 125–132. <https://doi.org/10.1016/j.ecss.2006.04.009>.
- Wu, H., Zhu, J.R., Choi, B.H., 2010. Links between saltwater intrusion and subtidal circulation in the Changjiang Estuary: a model-guided study. *Cont. Shelf Res.* 30 (17), 1891–1905. <https://doi.org/10.1016/j.csr.2010.09.001>.
- Wu, H., Zhu, J.R., Shen, J., Wang, H., 2011. Tidal modulation on the Changjiang River plume in summer. *J. Geophys. Res. Atmospher.* 116 (C8), 192–197. <https://doi.org/10.1029/2011JC007209>.
- Xue, P.F., Chen, C.S., Ding, P.X., Beardsley, R.C., Lin, H.C., Ge, J.Z., Kong, Y.Z., 2009. Saltwater intrusion into the Changjiang River: a model-guided mechanism study. *J. Geophys. Res. Oceans* 114 (C2). <https://doi.org/10.1029/2008JC004831>.
- Zhu, J.R., 2003. Ocean numerical calculation method and numerical model. China Ocean Press, Beijing (in Chinese with English Abstract).
- Zhu, J.R., Wu, H., Li, L., Wang, B., 2010. Saltwater intrusion in the Changjiang Estuary in the extremely drought hydrological year 2006. *J. East China Normal Univ. (Nat. Sci.)* 4 (1), 1–6 [in Chinese with English abstract].
- Zhu, J.R., Bao, D.Y., 2016. The effects of river regime changes in the Changjiang Estuary on hydrodynamics and salinity intrusion in the past 60 years I river regime changes. *Acta Oceanologica Sinica* 38 (12), 11–22. <https://doi.org/10.3969/j.issn.0253-4193.2016.12.002>.
- Zhu, J.R., Ding, P.X., Zhang, L.Q., Wu, H., Cao, H.J., 2006. Influence of the deep waterway project on the Changjiang Estuary. In: *The environment in Asia Pacific harbours* (pp. 79–92). Springer Netherlands. https://doi.org/10.1007/1-4020-3655-8_6.
- Zhu, J.R., Wu, H., Li, L., 2015. Hydrodynamics of the Changjiang Estuary and Adjacent Seas. In: *Ecological Continuum from the Changjiang (Yangtze River) Watersheds to the East China Sea Continental Margin* (pp. 19–45). Springer International Publishing. https://doi.org/10.1007/978-3-319-16339-0_2.
- Zhu, J.R., Yang, L.H., Zhu, S.X., 2002. Improvement of the stability of the estuarine coastal ocean model by a predictor-corrector scheme. *Oceanologia Et Limnologia Sinica* 33 (1), 15–22 [in Chinese with English abstract].